Philippine Journal of Science
154 No. 1: 169-178, February 2025
ISSN 0031 - 7683
Date Received: 08 Aug 2024

Chlorophyll-*a* Enhancement Induced by Monsoonal Island Wakes in the Western Region of Camiguin Island, the Philippines

Janell Carmina A Sihay[1]*, Cristy S. Acabado[2], and Cesar L. Villanoy[1]

[1]Marine Science Institute, University of the Philippines Diliman, Quezon City, National Capital Region 1101 the Philippines
[2]Institute of Marine Fisheries and Oceanology, College of Fisheries and Ocean Sciences, University of the Philippines Visayas, Miag-ao, Iloilo 5023 the Philippines

Satellite-derived observations of chlorophyll-*a* (Chl-*a*) concentration reveal patterns of enhancement, particularly at the west side of Camiguin Island in Bohol Sea, the Philippines. Previous studies have linked basin-scale chlorophyll variability with interannual rainfall anomalies due to the El Niño–Southern Oscillation. However, the role of other mesoscale processes such as upwelling, eddies, and island effects remains unexplored. Here, we analyzed ocean data to determine the related processes to the observed enhancement. We determined the spatiotemporal variability and distribution of Chl-*a* in the Bohol Sea. We found that Chl-*a* varies most on the seasonal scale following monsoon forcing. The west Camiguin enhancement is prominent during the northeast monsoon (NEM). We found that strong NEM winds drive mixing, upwelling, and particle entrainment (*i.e.* Chl-*a* as a proxy for phytoplankton). The monsoonal physical processes create favorable conditions for finer-scale enhancement through island wakes generated from the interaction of winds and currents with Camiguin Island.

Keywords: Bohol Sea, island mass effect, island wake, oceanic von Kármán vortex street

INTRODUCTION

Chlorophyll-*a* (Chl-*a*) is a photosynthetic pigment widely used as a proxy for phytoplankton. Synoptic observation of this pigment through satellite remote sensing reveals distribution patterns strongly linked with physical ocean processes and conditions across spatiotemporal scales (Mann 1992; Daly 1993). The physical ocean phenomena drive upper ocean mixing that determines the availability of light and nutrients (Sathyendranath *et al.* 2019). Most of the Chl-*a* variability has been observed at the mesoscale (10–100 km, seasonal to interannual; Talley *et al.* 2011; Du *et al.* 2023) and forced by processes such as eddies, upwelling, fronts, internal waves, and island wake effects (Vance and Doel 2010).

Camiguin Island is a pearl-shaped volcanic island within the Bohol Sea (8–10° N, 123–126° E, Figure 1). It spans a length of about 20 km across and has the highest elevation at 1,552 m. North of the island is a prominent westward current dubbed the Bohol Jet. This current connects the Pacific Ocean and the Sulu Sea and is coupled to a cyclonic eddy in the western Bohol Sea called the Iligan eddy (Gordon *et al.* 2011). Previous observations on the Chl-*a* concentrations in the Bohol Sea reveal interannual patterns of enhancement linked to El Niño–Southern Oscillation (ENSO) (Cabrera *et al.* 2011), particularly in the west of Camiguin Island. This appears to taper

*Corresponding author: jsihay@msi.upd.edu.ph

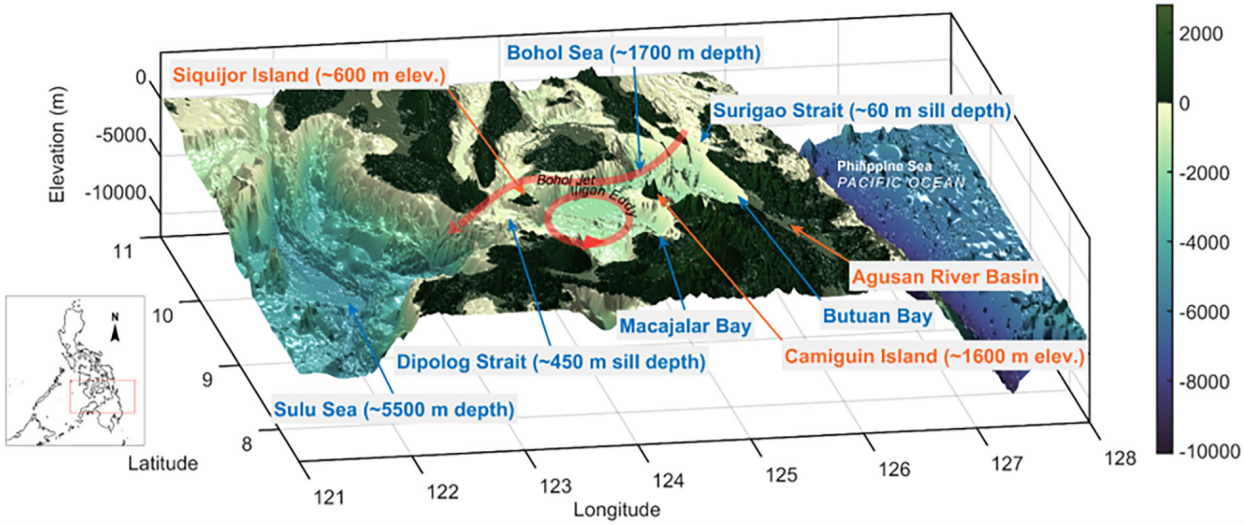

Figure 1. Bohol Sea 3-dimensional bathymetric map. Bathymetry data was retrieved from the GEBCO Compilation Group.

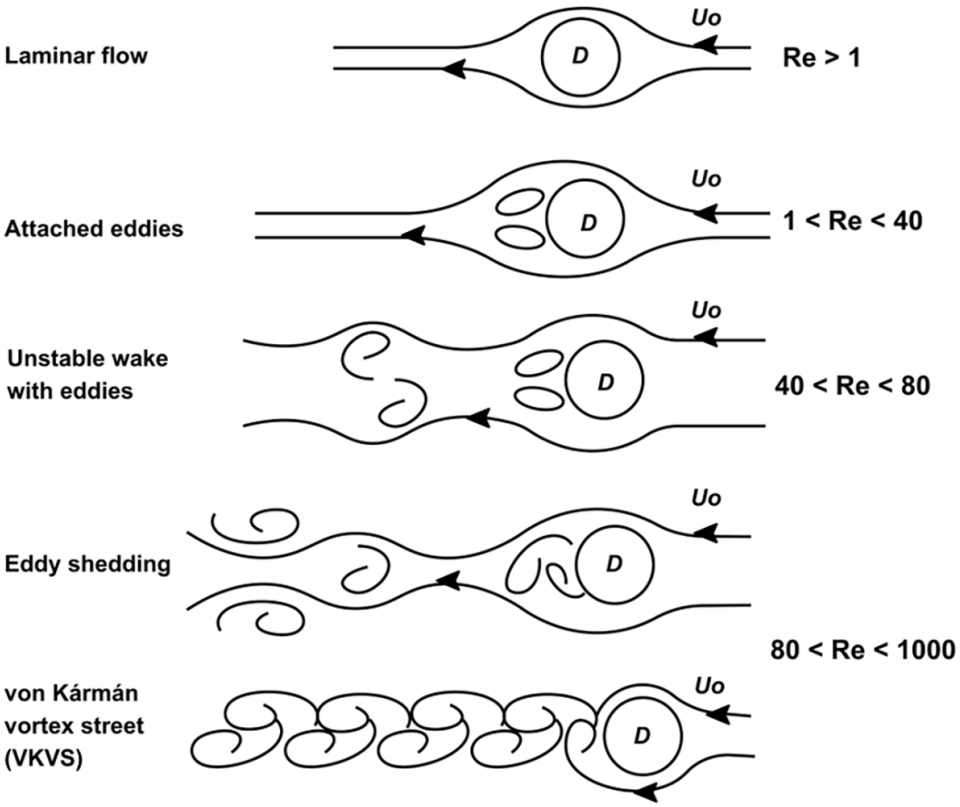

Figure 2. Various forms of wakes based on Reynold's number (R_e). U_o represents the incoming flow velocity, and D represents the island diameter. Illustration based on the studies by Frajka-Williams (2019) and Caldeira (2019).

northwest, a pattern characteristic of island wakes. We hypothesize that this pattern is a case of an island wake-induced enhancement.

Island wakes are defined as the changes in flow resulting from the interaction of an island with winds (resulting in atmospheric island wakes), currents (oceanic island wakes), or the interaction of both (atmospheric-induced oceanic island wakes; Caldeira 2019). Based on numerical studies on a cylindrical island, the resulting modified flows take various forms depending on the velocity of the flows and the shape of the island, a relationship described and simplified by the island wake parameter that is based on Reynold's number (*Re*; Tomczak 1998). When $Re < 1$, friction dominates resulting in a laminar flow (Figure 2). When $1 < Re < 40$, two steady eddies form on the leeward side of the island. When $40 < Re < 80$, the wake becomes unstable, resulting in the shedding of eddies. A von Karman street vortex (VKSV) occurs when $80 < Re < 1000$ (Frajka-Williams 2019; Caldeira 2019).

Wakes contribute to the enhanced phytoplankton biomass near islands, a phenomenon known as the island mass effect (Doty and Oguri 1956; de Falco *et al.* 2022). The island wakes physically resupply nutrients to the upper layers of the ocean through upwelling and eddies, resulting in increased primary production. It may also cause an island mass effect without new production through the uplifting and diffusion of the deep Chl-*a* maximum (Hasegawa *et al.* 2008, 2009).

In the present study, we analyze satellite ocean data to determine whether the enhancement is a result of island wakes by investigating the corresponding mesoscale physical oceanographic conditions and processes. Moreover, this study investigates the basin-scale spatiotemporal variability of monthly Chl-*a* and sea surface wind data in the Bohol Sea to determine the underlying ocean-atmosphere dynamics prior to conducting an island-scale investigation of Chl-*a* enhancement.

MATERIALS AND METHODS

Bohol Sea Chl-*a* and Sea Surface Winds Variability Analysis

The Chl-*a* data used in this study is the Global Ocean Colour (Copernicus-GlobColour) Bio-Geo-Chemical, L4 product (Product ID: OCEANCOLOUR_GLO_BGC_L4_MY_009_104), which provides monthly and interpolated values derived from multiple satellite instruments – including SeaWiFS, MODIS, MERIS, VIIRS-SNPP and JPSS1, and OLCI-S3A and S3B. Gridded monthly composite Chl-*a* data (Dataset ID: cmems_obs-oc_glo_bgc-plankton_my_l4-multi-4km_P1M) within the Bohol Sea region (8–10°N, 123–126°E) was obtained from the Copernicus Marine Service (http://marine.copernicus.eu), covering the period from September 1997–September 2023, maximizing the earliest available data of the product up to the time of analysis. The dataset's spatial resolution is 4 km and represents the mass concentration of Chl-*a* in seawater in mg m^{-3}. To analyze spatiotemporal variability, we applied empirical orthogonal function (EOF) analysis using the *eof* Python package (Dawson 2016).

To explore associated ocean-atmosphere variability, we analyzed the climatological mean sea surface winds over the Bohol Sea during January and July to represent the northeast monsoon (NEM) and southwest monsoon (SWM), respectively. Monthly wind velocity data (northward and eastward components in m s^{-1}) were retrieved from the Global Ocean Monthly Mean Sea Surface Wind and Stress product (Product ID: WIND_GLO_PHY_CLIMATE_L4_MY_012_003) from the Copernicus Marine Service (http://marine.copernicus.eu), spanning October 2007–October 2022 with a 0.25° spatial resolution (~ 25 km). This dataset consolidates ECMWF ERA5 reanalysis and scatterometer observations from Metop-A, B, and C satellites. Wind stress, stress curl, and Ekman transport and vertical velocities were computed using the MATLAB Climate Data Toolbox (Greene *et al.* 2019) to estimate wind-driven surface circulation patterns.

Island-scale Observations

To summarize the occurrence, location, and magnitude of west Camiguin enhancement, we utilized the gridded monthly composite Chl-*a* data and computed the difference of the area-averaged west (9.10345–9.27765°N, 124.80537–124.98046°E) and east Camiguin (9.10209–9.27630°N, 124.62822–124.45312°E). Positive values suggest an enhancement in west Camiguin, whereas negative values suggest an enhancement in east Camiguin. We also retrieved the Niño 3.4 Sea Surface Temperature time series from Reanalysis data product (Product ID: GLOBAL_OMI_CLIMVAR_enso_sst_area_averaged_anomalies) from 1997–2023 and the CPC Global Unified Gauge-Based Analysis of Daily Precipitation dataset from National Oceanic and Atmospheric Administration (NOAA) Physical Sciences Laboratory (PSL) to compare the Chl-*a* time series to climate and seasonal oscillations.

Then, we explored synthetic aperture radar (SAR) images taken by Sentinel-1 of west Camiguin using the Sentinel Hub EO Browser (https://apps.sentinel-hub.com/eo-browser/). SAR measures sea surface roughness and is widely used in the characterization of oceanic features – including eddies, fronts, wakes, wind-driven currents, and waves. We also explored daily composites of a higher

resolution Chl-*a* product (300-m spatial resolution) with a lower processing level (Level 3; Dataset ID: cmems_obs-oc_glo_bgc-plankton_my_l3-olci-300m_P1D), as these have not gone interpolation techniques to cross-check whether identified SAR image patterns manifested in the Chl-*a* distribution.

The circular shape of Camiguin Island allows us to theoretically estimate the characteristic flow; thus, we computed the island wake parameter (Equation 1) to confirm whether wakes can form. The island wake parameter is given by Equation 1 (Tomczak 1988):

$$Re = \frac{U_o h^2}{vD} \quad (1)$$

where U_o is the incoming flow velocity, h is the height of the water column, D is the island diameter, and v is the vertical eddy diffusivity.

For the upstream velocity estimates, we used the eastward seawater velocity and northward seawater velocity variables from the monthly dataset (cmems_mod_glo_phy_my_0.083_P1M-m) of Global Ocean Physics Reanalysis (Product ID: GLOBAL_MULTIYEAR_PHY_001_030) product.

RESULTS

Chlorophyll-*a* (Chl-*a*) Variability in Bohol Sea

The EOF results showed that the largest mode of variability in the Chl-*a* dataset (58.14%) is an annual oscillation (Figure 3a) of a spatial pattern west of Camiguin (dark red in Figure 3b). This pattern extends westward to Siquijor Island and out to the Sulu Sea. Chl-*a* in this specific area increases around January and decreases around July, which coincides with the NEM patterns in the Bohol Sea region. The 26-yr climatological mean of January revealed

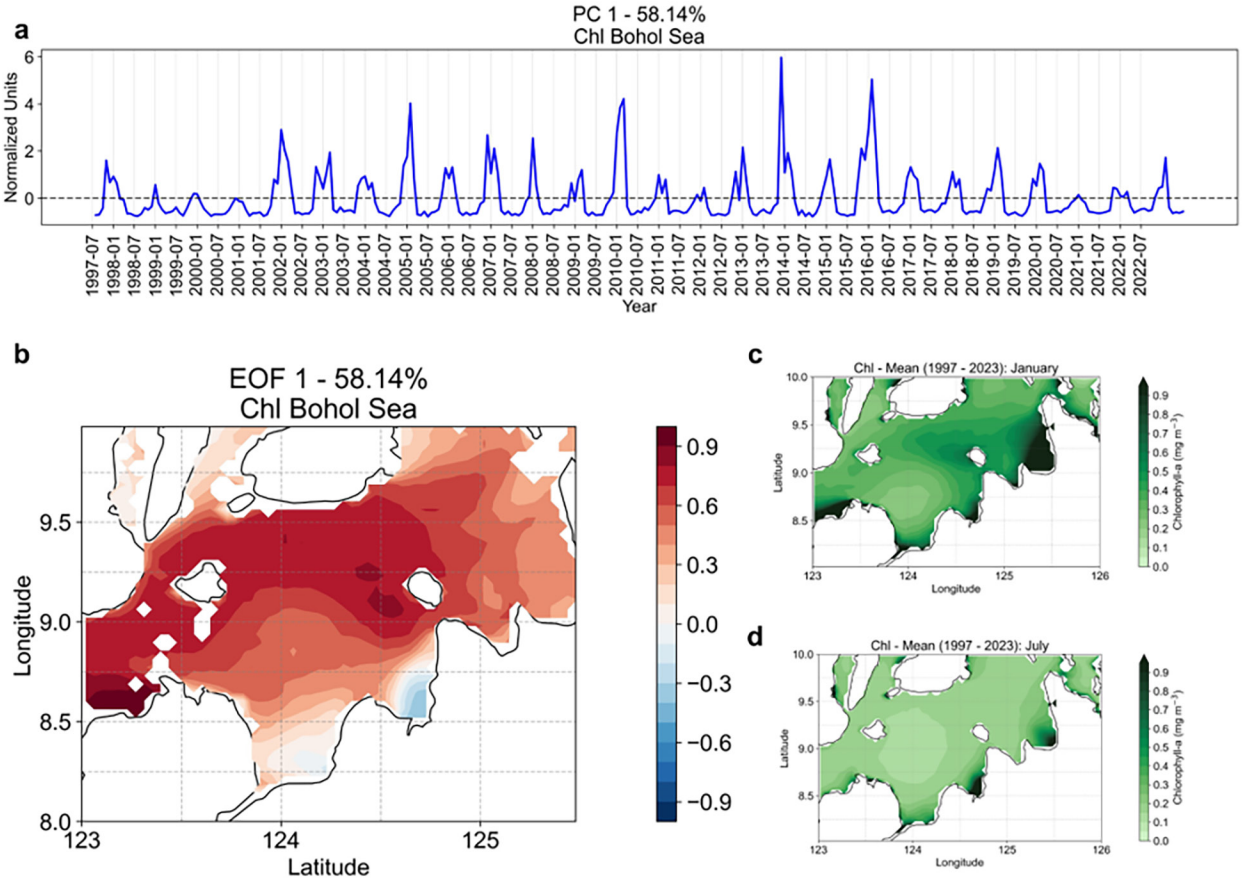

Figure 3. Spatiotemporal variability of chlorophyll-*a* (Chl-*a*) concentration in the Bohol Sea. The first mode, explaining 58.14% of the variability in the 26-yr monthly dataset, shows a seasonal oscillation (a) and a prominent spatial pattern (dark red) in the northwestern part of Bohol Sea (b). The climatological map of Chl-*a* in January reveals a distinct pattern west of Camiguin Island that extends westward to Siquijor Island (c), which is not observed in July (d). Chl-*a* data provided by the EU Copernicus Marine Service Information (CMEMS).

a clearly defined wake-like spatial pattern (Figure 3c) which was not observed in July (Figure 3d).

Seasonal Sea Surface Wind Dynamics

We observed that wind stress vectors were stronger during the NEM (Figure 4a, black vectors) than in the SWM (Figure 4b, black vectors). During the NEM, the wind stress acts in the same direction as the Bohol Jet (Figure 4a). In both seasons, we observed increased wind stress over the basin relative to the outside of the Bohol Sea, a pattern suggesting orographic steering and wind jet effect. These are likely generated when large-scale prevailing winds, *i.e.* the northeast and southwest winds, are intensified as they are funneled through Surigao and Dipolog Straits, respectively.

During NEM, Ekman transport is northwestward (Figure 4a, red vectors). During the SWM, the Ekman transport is southeastward, with smaller transport than during the NEM (Figure 4b, red vectors).

The fastest vertical velocities were observed during the NEM (Figure 4a, filled contour). Maximum upwelling rates were calculated at the lee of Camiguin at 133 m mo^{-1}, whereas maximum downwelling rates of 120 m mo^{-1} were observed near Negros and Bohol Island (Figure 4b). The Ekman vertical velocities were relatively slower during the SWM, estimated at only about 30 m mo^{-1}.

West Camiguin Chl-*a* Enhancement Pattern

We found two images showing a VKSV pattern (Figure 5). These were taken on 03 Dec 2015 and 11 Mar 2020. We calculated the shallow island wake parameter (Equation 1) using the NEM mean current velocity to confirm whether the observed features in the SAR images are likely to be a VKSV pattern.

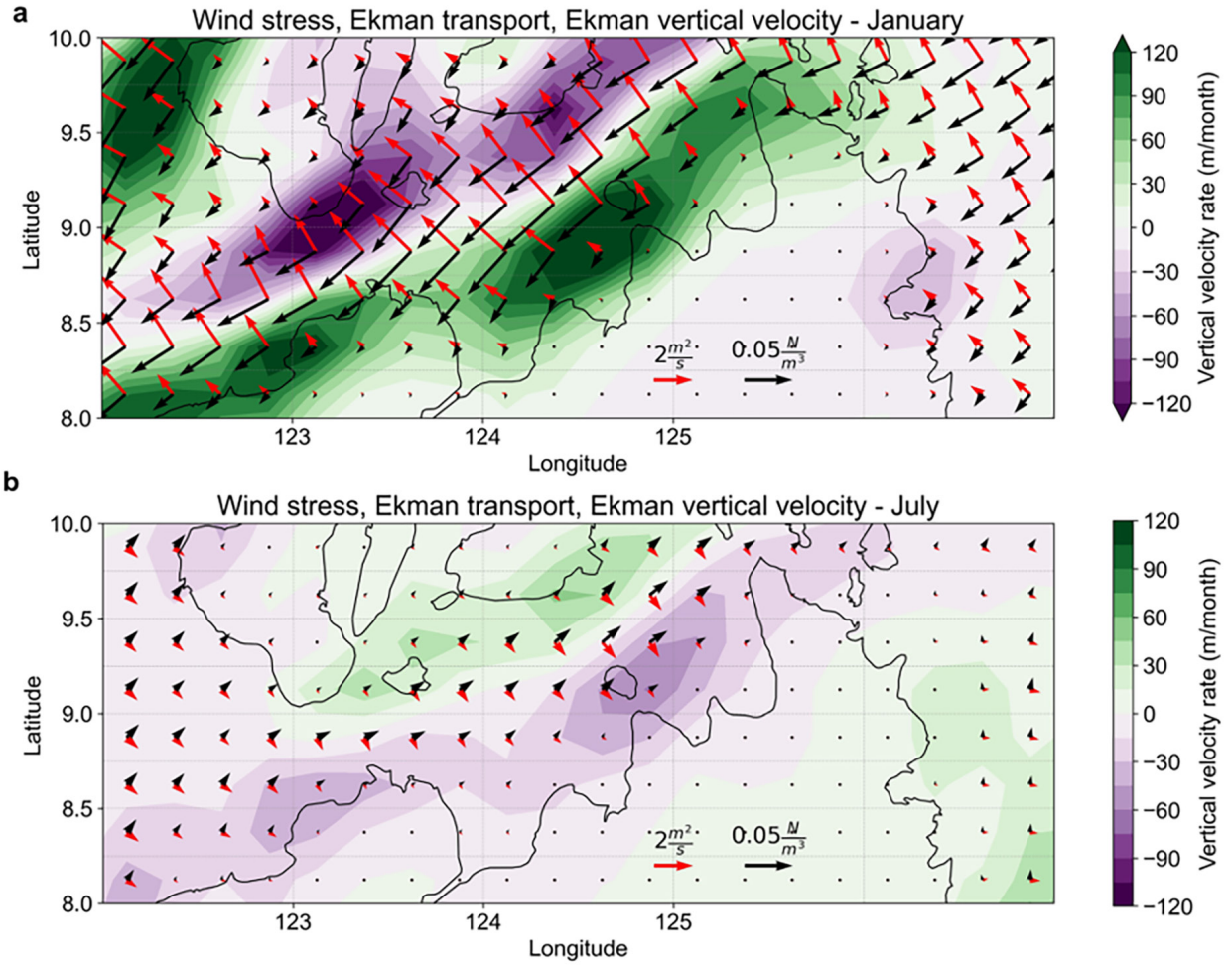

Figure 4. Mean wind stress (black vectors), Ekman transport (red vectors), and Ekman vertical velocity (filled contour) during the NEM (a) and SWM (b). The green (purple) contour shading shows upwelling (downwelling). Wind stress, Ekman transport, and Ekman vertical velocity computed from the global ocean monthly mean sea surface wind and stress from Scatterometer and model product by EU Copernicus Marine Service Information (CMEMS).

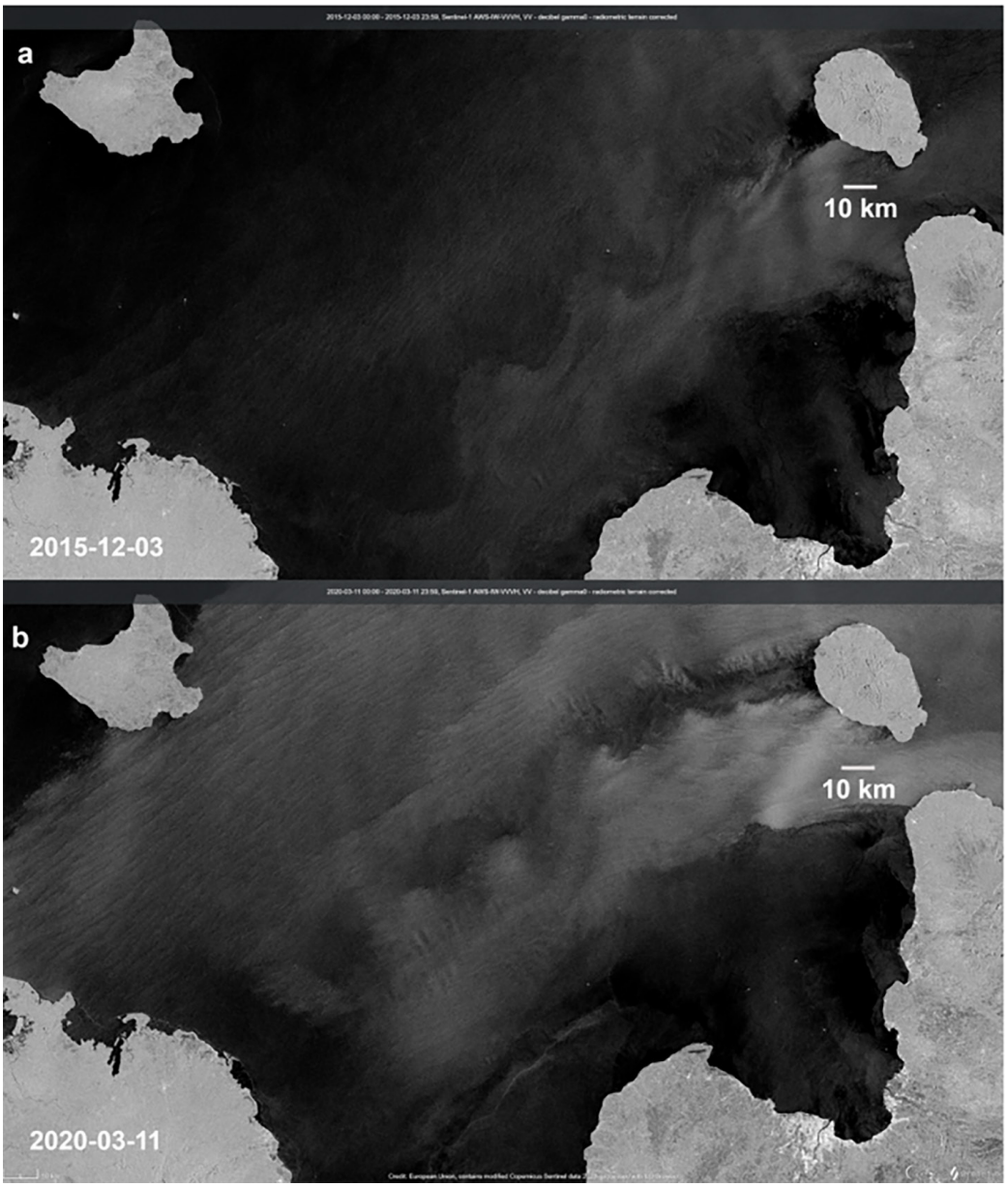

Figure 5. SAR images showing von Karman street vortex (VKSV), eddy shedding-like patterns. Images retrieved from the Copernicus Sentinel data (European Union) were processed with the Sentinel hub EO Browser.

The diameter of Camiguin Island was estimated at 22.5 km. The mean velocity upstream of Camiguin Island during NEM was 0.05 m s^{-1}. The vertical eddy viscosity was 0.0001 m^2 s^{-1} (vertical eddy diffusivity global average). The height of the water column that was used is 200 m. Given this, we computed a *Re* of 960.49. This means that in theory, VKSV and eddy shedding may occur during the NEM.

To confirm whether these flows correspond to Chl-*a* enhancement patterns, we explored Level 3 data products. The Level 3 Chl-*a* data from 10 Mar 2020 was available but did not show a vortex street-like pattern. We did, however, find Level 3 data from other dates showing vortex-street-like wakes. These were taken on 24 and 25 Feb 2021 (Figure 6).

The time series of the Chl-*a* difference revealed that the strongest west Camiguin enhancements occurred during 2003–2004, 2004–2005, 2009–2010, and 2015–2016, which were all recorded El Niño events (Figure 7a). NEM enhancements during La Nina events occurred during 1999–2000, 2007–2008, and 2010–2011. East Camiguin enhancements occurred in La Niña and neutral phases, but these were not as notable in magnitude compared to west Camiguin enhancements.

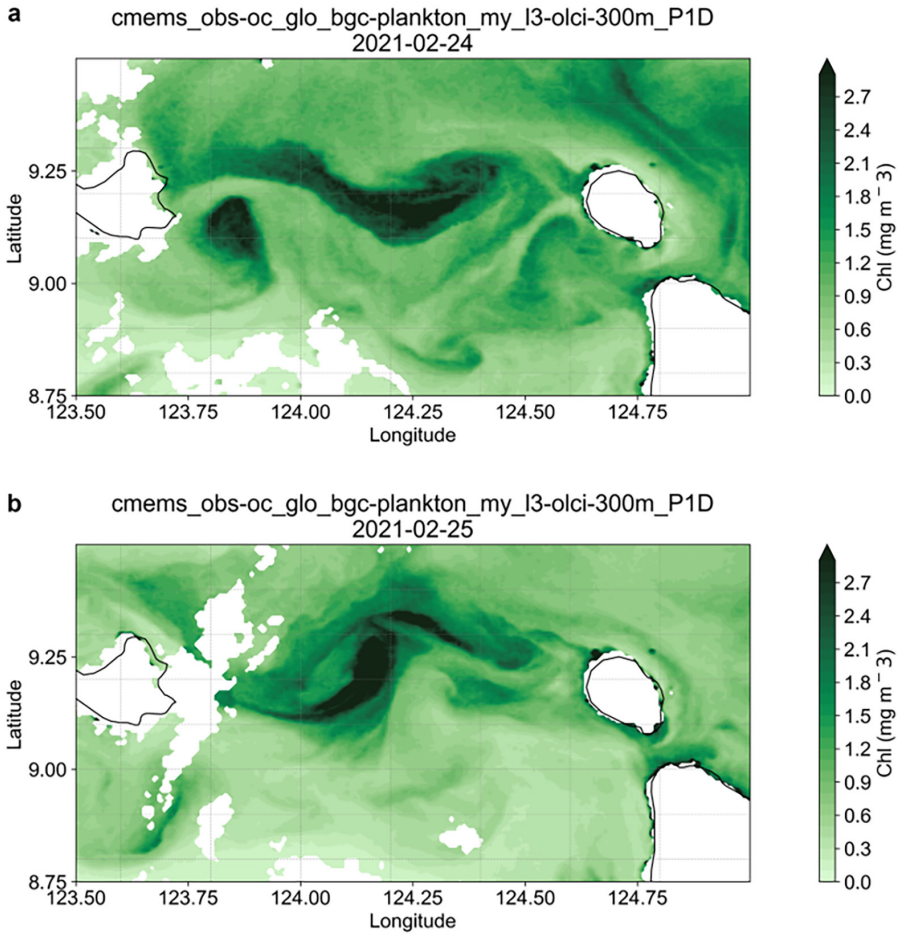

Figure 6. Level 3 Chl-*a* data on 24 Feb 2021 (a) and 25 Feb 2021 (b). Source: Global Ocean Colour (Copernicus-GlobColour), Bio-Geo-Chemical, L3 (daily) from Satellite Observations (1997–ongoing). EU Copernicus Marine Service Information (CMEMS) Marine Data Store (MDS).

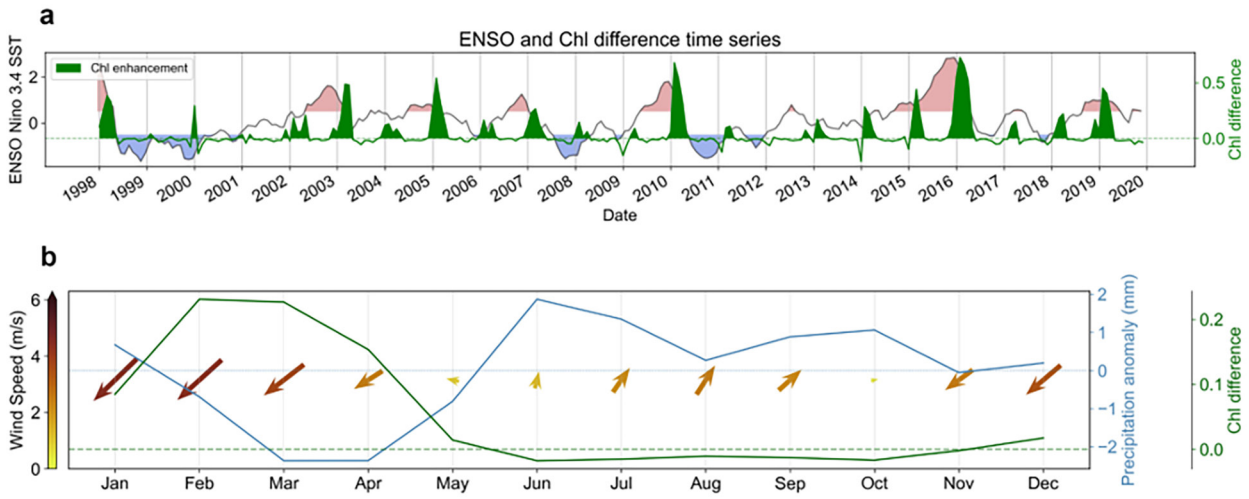

Figure 7. Time series of Nino 3.4 SST Index and Chl-*a* difference between the west and east of Camiguin Island (a) and time series of monthly climatology of Chl-*a* difference, mean wind vectors, and precipitation anomaly in Bohol Sea (b). Positive values correspond to west Camiguin Chl-*a* being greater than east Camiguin Chl-*a*, whereas negative values correspond to west Camiguin Chl-*a* being less than east Camiguin Chl-*a*. Chl-*a* and ENSO Index data was provided by the EU Copernicus Marine Service Information (CMEMS). Precipitation was retrieved from NOAA PSL, Boulder, CO, USA.

Comparing the Chl-*a* difference with monsoon dynamic factors, *i.e.* rainfall and winds (Figure 7b), Chl-*a* difference peaks were observed in February and March when negative rainfall anomalies were recorded, and northeast winds were strong. The enhancements in east Camiguin were observed during positive rainfall anomalies associated with weaker southwest winds.

DISCUSSION

The seasonal monsoon wind drives most of the Chl-*a* variability in Bohol Sea. Chl-*a* is enhanced during the NEM and reduced during the SWM. The west Camiguin enhancement pattern only appears during NEM, which means that this pattern is driven primarily by NEM winds and the associated ocean-atmosphere processes such as wind-driven currents and rainfall patterns.

Similar to wind jets described by Pullen *et al.* (2008) and Rypina *et al*. (2010), the narrow confines of Surigao Strait funnel large-scale NEM winds into the basin, creating strong winds that impart stress over the Bohol Sea surface. Stronger wind stress may overcome stratification and transfer energy deeper into the water column, reaching the deep Chl-*a* maximum and the nutricline. In turn, this can promote primary production as nutrients reach the well-lit layers. Similar cases of this wind forcing-induced enhancement were observed in Chl-*a* variability studies of the western tropical Pacific (Hou *et al.* 2016) and the South China Sea (Zhang *et al*. 2016; Chen *et al.* 2020). In the Philippines, wind jets between Panay and Mindoro Islands during the NEM induce upwelling through the formation of a cyclonic eddy from the positive wind stress curl at the lee of Panay (Amedo-Repollo *et al.* 2019).

The NEM winds strengthen the Bohol Jet in two ways. First, through direct frictional forces, where the wind stress acts in the same direction as the westward throughflow. Second, through the geostrophic balance, where the pressure gradient force is balanced by the Coriolis. The sustained wind stress drives a northwestward Ekman transport, as Coriolis acts to the right of the northeast winds. The water accumulates and builds pressure in the northern half of the basin. Currents would then be supposed to flow from high to low pressure (north to south), but the Coriolis once again acts on these flows and deflects them to the right. This results in a current moving westward, which is already the direction of the Bohol Jet, resulting from the larger scale pressure difference between the neighboring basins, the Pacific and Sulu Sea. Therefore, the NEM winds increase the meridional pressure gradient force within the basin, intensifying the Bohol Jet through geostrophic even further.

Another consequence of the northwestward Ekman transports is upwelling and downwelling regions to satisfy the conservation of mass. These areas may be determined from the relative position of the wind with respect to a coastal boundary. In a basin like the Bohol Sea, the northwestward Ekman transport of the NEM would result in coastal upwelling in the northern Mindanao bays and Camiguin Island, while causing downwelling in the coastal regions of Bohol and Negros Island. This is similar to the coastal upwelling described in the nearby northern Zamboanga Peninsula (Villanoy *et al.* 2011) and the South China Sea (Yu *et al.* 2019).

The upwelling in the southern half and downwelling in the northern half of Bohol Sea during the NEM is also evidenced by the Ekman vertical velocity estimates, computed from the curl of the wind stress field. The vertical velocity estimates reach 120 m mo^{-1}, which is deeper than the reported range of *in situ* measurements of the deep chlorophyll maximum (20–50 m) in the Bohol Sea (Cabrera *et al.* 2011). This means that aside from mixing from wind stress and the offshore Ekman transport to the northwest, the vertical Ekman motion due to wind stress curl could be another mechanism that explains the observed enhancement at the surface on a basin scale.

While there is a Bohol Sea basin-scale Chl-*a* enhancement occurring during the NEM, the pattern observed in west Camiguin may also be attributed to island-scale wake effects. The SAR images and the island wake parameter estimate suggest the potential occurrence of eddy shedding or vortex-street flows resulting from the interaction of NEM currents with the island, similar to island wake studies conducted in Didicas Island in Luzon (Liu *et al*. 2022) and Green Island in Taiwan (Liu and Chang 2018; Hsu *et al.* 2019).

The Chl-a aggregation around Camiguin Island may have originated from upstream sources, such as from the Agusan River, as they are "trapped" on the leeward side of Camiguin due to pressure differences. Alternatively, it could be indicative of new production resulting from upwelled nutrients or sourced from the deep chlorophyll maximum (Hasegawa *et al.* 2008, 2009; Hsu *et al.* 2019).

The island wake-induced enhancements are particularly favorable during the NEM and ENSO. During these periods, the water column is less stratified, and the Bohol Jet intensifies, thereby enhancing upwelling and particle entrainment processes. The NEM winds drive either southwestward or northwestward transport, interacting with Camiguin Island and forming vortex-street wakes.

CONCLUSION

Our study set out to determine the mesoscale ocean conditions and processes related to the Chl-*a* enhancement west of Camiguin Island in the Bohol Sea. We found the Chl-*a* in the basin varies most on a seasonal scale, following monsoon forcing. In addition, strong NEM winds drive strong mixing and entrainment from the intensified Bohol Jet from frictional forces, geostrophy, and Ekman dynamics. Furthermore, we found evidence that island wakes occur from the interaction of winds and currents with the island of Camiguin and that the observed Chl-*a* enhancement was only favorable during the NEM conditions. This is the first study describing the Camiguin Island wake and its relationship and potential influence on Chl-*a* enhancement. Long-term *in situ* observations of this phenomenon will help describe the fine-scale evolution of the wakes and their role in the interconnectivity and productivity within the Bohol Sea.

ACKNOWLEDGMENTS

Janell Sihay thanks the Philippine Department of Science and Technology–Accelerated Science and Technology Human Resource Development Program for providing the scholarship that supported this research. Special thanks to Dr. Charina Lyn Amedo-Repollo and the Physical Oceanography Laboratory of the University of the Philippines Marine Science Institute for their guidance and support throughout this study. The authors acknowledge the anonymous reviewers for their critical insights and thoughtful suggestions, which significantly improved the quality of this paper.

REFERENCES

AMEDO-REPOLLO CL, FLORES-VIDAL X, CHAVANNE C, VILLANOY CL, FLAMENT P. 2019. Low-frequency surface currents and generation of an island lee eddy in Panay Island, Philippines. Journal of Physical Oceanography 49(3): 765–787.

CABRERA O, VILLANOY C, DAVID L, GORDON A. 2011. Barrier layer control of entrainment and upwelling in the Bohol Sea, Philippines. Oceanography 24(01): 130–141.

CALDEIRA RMA. 2019. Island wakes. In: Encyclopedia of Ocean Sciences. Elsevier. p. 83–91.

DE FALCO C, DESBIOLLES F, BRACCO A, PASQUERO C. 2022. Island mass effect: a review of oceanic physical processes. Frontiers in Marine Science 9: 894860.

[EU CMEMS MDS] EU Copernicus Marine Service Information Marine Data Store. n/d. Global ocean colour (Copernicus-GlobColour), bio-geo-chemical, L4 (monthly and interpolated) from satellite observations (1997–ongoing). Accessed in December 2022 at https://doi.org/10.48670/moi-0028

[EU CMEMS MDS] EU Copernicus Marine Service Information Marine Data Store. n/d. Global ocean hourly sea surface wind and stress from scatterometer and model. Accessed in December 2022 at https://doi.org/10.48670/moi-00305

[EU CMEMS MDS] EU Copernicus Marine Service Information Marine Data Store. n/d. Nino 3.4 sea surface temperature time series from reanalysis. Accessed in December 2022 at https://doi.org/10.48670/moi-00219

[EU CMEMS MDS] EU Copernicus Marine Service Information Marine Data Store. Global ocean physics reanalysis. Accessed in December 2022 at https://doi.org/10.48670/moi-00021

CHEN H-H, TANG R, ZHANG H-R, YU Y, WANG Y. 2020. Investigating the relationship between sea surface chlorophyll and major features of the South China Sea with satellite information. Journal of Visualized Experiments 160: 61172.

DALY KL. 1993. Physical-biological interactions influencing marine plankton production. Annual Review of Ecology and Systematics 24: 55–585.

DAWSON A. 2016. eofs: a library for EOF analysis of meteorological, oceanographic, and climate data. Journal of Open Research Software 4(1): 1.

OTY MS, OGURI M. 1956. The island mass effect. ICES Journal of Marine Science 22(1): 33–37.

DU Y, WANG F, WANG T, LIU W, LIANG L, ZHANG Y, CHEN Y, LIU J, WU W, YU K, ZHANG J. 2023. Multi-scale ocean dynamical processes in the Indo-Pacific Convergence Zone and their climatic and ecological effects. Earth-Science Reviews 237: 104313.

FRAJKA-WILLIAMS E. 2019. Topographic eddies. In: Encyclopedia of Ocean Sciences. Elsevier. p. 158–168.

[GEBCO] General Bathymetric Chart of the Oceans Compilation Group. 2023. GEBCO 2023 grid. Accessed at https://www.gebco.net/data_and_products/gridded_bathymetry_data/

GORDON A, SPRINTALL J, FFIELD A. 2011. Regional oceanography of the Philippine archipelago. Oceanography 24(01): 14–27.

GREENE CA, THIRUMALAI K, KEARNEY KA, DELGADO JM, SCHWANGHART W, WOLFENBARGER NS, THYNG KM, GWYTHER DE, GARDNER

AS, BLANKENSHIP DD. 2019. The climate data toolbox for MATLAB. Geochemistry, Geophysics, Geosystems 20(7): 3774–3781.

HASEGAWA D, LEWIS MR, GANGOPADHYAY A. 2009. How islands cause phytoplankton to bloom in their wakes. Geophysical Research Letters 36(20): 2009GL039743.

HASEGAWA D, YAMAZAKI H, ISHIMARU T, NAGASHIMA H, KOIKE Y. 2008. Apparent phytoplankton bloom due to island mass effect. Journal of Marine Systems 69(3–4): 238–246.

HOU X, DONG Q, XUE C, WU S. 2016. Seasonal and interannual variability of chlorophyll-*a* and associated physical synchronous variability in the western tropical Pacific. Journal of Marine Systems 158: 59–71.

HSU P-C, CHENG K-H, JAN S, LEE H-J, HO C-R. 2019. Vertical structure and surface patterns of Green Island wakes induced by the Kuroshio. Deep Sea Research Part I: Oceanographic Research Papers 143: 1–16.

LIU C, CHANG M. 2018. Numerical studies of submesoscale island wakes in the Kuroshio. Journal of Geophysical Research: Oceans: 123(8): 5669–5687.

LIU F, LIU Y, TANG S, LI Q. 2022. Oceanic Kármán vortex streets in the Luzon Strait in the lee of Didicas Island from multiple satellite missions. Remote Sensing 14(17): 17.

MANN KH. 1992. Physical influences on biological processes: how important are they? South African Journal of Marine Science 12(1): 107–121.

[NOAA PSL] National Oceanic and Atmospheric Administration Physical Sciences Laboratory. CPC global unified gauge-based analysis of daily precipitation. Accessed in December 2022 at https://psl.noaa.gov/data/gridded/data.cpc.globalprecip.html

PULLEN J, DOYLE JD, MAY P, CHAVANNE C, FLAMENT P, ARNONE RA. 2008. Monsoon surges trigger oceanic eddy formation and propagation in the lee of the Philippine Islands. Geophysical Research Letters 35(7).

RYPINA II, PRATT LJ, PULLEN J, LEVIN J, GORDON AL. 2010. Chaotic advection in an archipelago. Journal of Physical Oceanography 40(9): 1988–2006.

SATHYENDRANATH S, PLATT T, BREWIN RJW, JACKSON T. 2019. Primary production distribution. In: Encyclopedia of Ocean Sciences. Elsevier. p. 635–640.

TALLEY LD, PICKARD GL, EMERY WJ eds. 2011. Descriptive physical oceanography: an introduction (6th ed). Academic Press.

TOMCZAK M. 1988. Island wakes in deep and shallow water. Journal of Geophysical Research: Oceans 93(C5): 5153–5154.

VANCE TC, DOEL RE. 2010. Graphical methods and Cold War scientific practice: the Stommel diagram's intriguing journey from the physical to the biological environmental sciences. Historical Studies in the Natural Sciences 40(1): 1–47.

VILLANOY CL, CABRERA OC, YÑIGUEZ AT, CAMOYING MG, ASUNCION B DE GUZMAN, DE GUZMAN A, DAVID LT, FLAMENT P, FLAMENT PJ. 2011. Monsoon-driven coastal upwelling off Zamboanga Peninsula, Philippines. Oceanography 24(1): 156–165.

YU Y, XING X, LIU H, YUAN Y, WANG Y, CHAI F. 2019. The variability of chlorophyll-*a* and its relationship with dynamic factors in the basin of the South China Sea. Journal of Marine Systems 200: 103230.

ZHANG W-Z, WANG H, CHAI F, QIU G. 2016. Physical drivers of chlorophyll variability in the open South China Sea: chlorophyll variability in the SCS. Journal of Geophysical Research: Oceans 121(9): 7123–7140.